J Therm Anal Calorim (2017) 129:147–159
DOI 10.1007/s10973-017-6116-8

Thermal, combustion and optical properties of new polyimide/ODA-functionalized Fe_3O_4 nanocomposites containing xanthene and amide groups

Meisam Shabanian[1] · Zeinab Mirzakhanian[1] · Hassan Moghanian[2] · Mohsen Hajibeygi[3] · Hamid Salimi[1] · Hossein Ali Khonakdar[4]

Received: 22 July 2016 / Accepted: 22 January 2017 / Published online: 6 February 2017

Abstract A new soluble polyimide was successfully synthesized via direct poly-condensation reaction between aromatic diamine containing xanthene group and aliphatic dianhydride. Multifunctional polyimide including xanthene derivatives, amide groups and high content of aromatic rings as well as aliphatic linkages was designed and synthesized. The polyimide was characterized by size exclusion chromatography, Fourier transform infrared spectroscopy and nuclear magnetic resonance (^{1}H NMR). Fe_3O_4 nanoparticles were functionalized by 4,4′-oxydianiline (ODA). Polyimide/Fe_3O_4 nanocomposites were prepared by covalently embedding the ODA-functionalized Fe_3O_4 (ODA-Fe_3O_4) containing amine groups (5 and 8 mass% of the nanoparticle). This functionality not only gave specific characteristics to Fe_3O_4 nanoparticles but also improved the interphase interaction between the nanoparticles and the polyimide matrix through covalent attachment. For comparison, nanocomposites using unmodified Fe_3O_4 nanoparticles also were prepared. The TEM analysis showed better dispersion of ODA-Fe_3O_4 within the polyimide matrix, which arising from formation of covalent bonding between ODA-functionalized Fe_3O_4 and the polyimide chains. Moreover, magnetic, optical, combustion and thermal properties of the polyimide and the corresponding nanocomposites were studied. Thermo gravimetric analysis results indicated improving on thermal properties of the polyimide nanocomposites as compared with the neat polyimide. According to microscale combustion calorimetry (MCC) analysis, 73.5% reduction in the peak heat release rate value was achieved by introducing 8 mass% of ODA-Fe_3O_4 in the polyimide matrix. Moreover, MCC analysis showed that ODA-Fe_3O_4 have better efficiency on improving the flame retardancy of the polyimide as compare with unmodified Fe_3O_4 nanoparticles.

Keywords Polyimide nanocomposite · Fe_3O_4 nanoparticle · Xanthene · Magnetic study · Flammability

Introduction

Polymer nanocomposites have been recognized as one of the advanced materials due to their broad range of potential applications compared with those of neat polymer. Magnetic polymer nanocomposites combining the advantages of the magnetic nanoparticles and the multiple properties of the polymer matrix such as mechanical, thermal, barrier properties and flammability have opened a new gateway in developing nanocomposite systems with improved performances [1–3].

Fe_3O_4 showed special properties such as ease of synthesis, super paramagnetic, nontoxicity and biocompatibility [4]. Fe_3O_4 nanoparticles were used as an important material in various areas including catalyst, magnetic recording, magnetic resonance imaging (MRI), magnetic sensing, drug delivery systems and cancer therapy. Due to

✉ Meisam Shabanian
m.shabanian@standard.ac.ir

[1] Faculty of Chemistry and Petrochemical Engineering, Standard Research Institute, Karaj 31745-139, Iran

[2] Department of Chemistry, Dezful Branch, Islamic Azad University, Dezful, Iran

[3] Faculty of Chemistry, Kharazmi University, Tehran 15719-14911, Iran

[4] Department of Polymer Engineering, Faculty of Engineering, South Tehran Branch, Islamic Azad University, P.O. Box 19585-466, Tehran, Iran

large surface area-to-volume ratio and also magnetic dipole–dipole interaction, the Fe_3O_4 nanoparticles tend to agglomerate [5]. Significant attentions have been used toward the surface modification of magnetic nanoparticles with different methods to have better dispersion in polymer matrix. Surface modification of nanoparticles improved the interaction and compatibility of the nanoparticles with polymer matrix, which can further improve the quality of materials [6, 7].

Among many high-performance polymers, aromatic polyimides (PIs) were classified as high-performance polymers because of the combination properties such as high thermal resistance, excellent mechanical properties, low dielectric constant and high chemical resistance [8–10]. The high-performance polymers are interesting matrix for nanocomposites. However, poor solubility and high transition temperatures of polyimides limited their processing and application. Those drawbacks can be improved by several methods, such as introduction of flexible linkages [11, 12], bulky pendent substituents [9, 13–15] and aliphatic moieties [16] into the polyimide chain.

Xanthenes was found to be natural products [17] and known as leuco dyes [18], pH-sensitive fluorescent materials and in laser technologies [19] due to their useful spectroscopic properties. Xanthene derivatives were also used to design thermally stable aromatic polyamides [20]. Due to steric bulk of xanthene skeleton, the solubility of aromatic polymers could improve. Moreover, incorporated xanthene derivatives into polymer backbones as conjugation systems was a promising way to enhance liquid crystallinity, the photoluminescence (PL) and electroluminescence properties of the polymers [21, 22].

It is, thus, worthwhile to design polyimides containing xanthene group as a high-performance material.

The present study deals with the design and synthesis of a new PI containing xanthene and amide groups, and its subsequent nanocomposites with two different contents of Fe_3O_4 nanoparticles (5 and 8 mass%). Surface modification of Fe_3O_4 with ODA not only decreased the attraction forces between the nanoparticles and prevented agglomeration but also improved the interphase interaction with the PI matrix. The polyimide nanocomposites were characterized by Fourier transform infrared spectroscopy (FT-IR), X-ray diffraction (XRD), transmission electron microscopy (TEM), UV–Vis and fluorescence spectroscopy. The effect of Fe_3O_4 nanoparticles on magnetic properties, combustion and thermal properties of PI were investigated.

Experimental

Materials and measurements

4-Nitrobenzaldehyde, 3,5-xylenol, *p*-toluenesulfonic acid (*p*-TSA), hydrazine monohydrate 80%, triethylamine, *N,N*-dimethylacetamide (DMAc), ammonia, pyridine, solvents and epiclon [5-(2,5-dioxotetrahydro-3-furanyl)-3-methyl-3-cyclohexene-1,2-dicarboxylic anhydride] were purchased from Merck and used without further purification. Palladium on carbon (Pd/C) 10%, 3,5-dinitrobenzoyl chloride, $FeCl_3{\cdot}6H_2O$, $FeCl_2{\cdot}4H_2O$, 3-chloropropyl-trimethoxysilane(CPTS), 4,4′-oxydianilineobtained from Aldrich were used without further purification.

Monomer synthesis

Diamine (7) containing xanthenes group was synthesized through four step reactions according to the previous literature [23].

Synthesis of polyimide

Synthesis of polyimide via chemical method

0.5 mmol of diamine (7), 0.5 mmol of epiclon (8) and 5 mL of dried DMAc were added into 50-mL round-bottomed flask equipped with a magnetic stirrer under N_2 atmosphere and the reaction mixture was stirred at 25 °C for 6 h to produced polyamic acid (PAA). Then, a mixture of Ac_2O and pyridine (1 mL, volume ratio 2:1) was added to PAA solution, and the reaction mixture was stirred in oil bath at 80 °C for 24 h for chemical imidization. Subsequently, the obtained viscose solution was poured into 50 mL of cold methanol and the precipitated polymer was collected by filtration, washed four times with hot methanol and dried at 70 °C for 10 h in vacuum oven.

Synthesis of polyimide via thermal method

0.5 mmol of diamine (7), 0.5 mmol of epiclon (8) and 5 mL of dried DMAc were added into 50-mL round-bottomed flask equipped with a magnetic stirrer under N_2 atmosphere and the reaction mixture was stirred at 25 °C for 24 h to produced polyamic acid (PAA). The resulting PAA solution was cast into a glass plate and placed in a vacuum oven for a programmed heat treatment: 2 h at 70 °C, 2 h at 110 °C, 2 h at 170 °C, 4 h at 200 °C. Elemental analysis: calculated for $C_{43}H_{37}N_3O_6$, calculated: C, 74.66; H, 5.39; N, 6.07, found: C, 74.81; H, 5.51; N, 5.98.

Preparation of magnetic nanoparticles

Preparation of Fe_3O_4 magnetic nanoparticles

The Fe_3O_4 magnetite nanoparticles were prepared according to the literature [24]. Briefly, 4 mmol $FeCl_3{\cdot}6H_2O$ and 2 mmol $FeCl_2{\cdot}4H_2O$ were dissolved in 100 mL water. The solution was subsequently heated to 90 °C and N_2 was continuously purged in solution, for O_2 exhausting. 5 mL of concentrated ammonia (25%) were added quickly and the solution was stirred under N_2 for 1 h and then cooled to room temperature. The precipitate was separated by magnetic decantation and washed with deionized water and ethanol, respectively.

Preparation of silica-coated Fe_3O_4 nanoparticles (Fe_3O_4@SiO_2)

Fe_3O_4@SiO_2 nanoparticles were prepared using Stöber method [25]. The details were described as follows: Fe_3O_4 nanoparticles (0.5 g) were dispersed in the mixture of water (80 mL) and ethanol (15 mL). After that, the mixture was irradiated with high-intensity ultrasonic wave for 15 min. Then the ammonia solution (2 mL, 25 mass%) and (tetraethylorthosilicate) TEOS (2 mL) were added to the mixture and mechanically stirred at room temperature for 12 h under N_2 atmosphere. The core–shell nanoparticles were separated from the reaction medium using a magnet, and then washed several times with water and ethanol and dried at 50 °C.

Synthesis of 3-chloropropyl-functionalized silica-coated Fe_3O_4 nanoparticles (Fe_3O_4@SiO_2–Cl)

Chloropropyl-modified silica-coated Fe_3O_4 nanoparticles were prepared according to the reported procedure [26]. 0.5 g of Fe_3O_4@SiO_2 nanoparticles was dispersed in 50 mL of toluene using an ultrasonic bath to produce a uniform suspension. 1 mL of 3-chloropropyl-trimethoxysilane (CPTS) was added to the mixture and was stirred for 24 h at 60 °C under N_2 atmosphere. Finally, the chloropropyl-functionalized Fe_3O_4@SiO_2–Cl nanoparticles were separated using an external magnet and dried in vacuum oven.

Oxydianiline-functionalized Fe_3O_4 magnetic nanoparticles (ODA-Fe_3O_4)

The ODA-Fe_3O_4 nanoparticles were prepared as following: 0.5 g Fe_3O_4@SiO_2–Cl nanoparticles were dispersed in 50 mL dry toluene under N_2 atmosphere. 5 mmol of 4, 4′-oxydianiline and 5 mmol of triethylamine were added to mixture and were agitated vigorously in reflux conditions for 48 h. The solid material was obtained by magnetic separation and washed with toluene and ethanol followed by drying at 80 °C for 6 h in vacuum oven.

Preparation of polyimide/Fe_3O_4 nanocomposites (PI/Fe_3O_4) (PIN-A) and polyimide/ODA-Fe_3O_4 nanocomposites (PI/ODA-Fe_3O_4) (PIN-B)

For the preparation of PI/Fe_3O_4 nanocomposites and PI/ODA-Fe_3O_4 nanocomposites, equimolar amount of diamine and dianhydrid (epiclon) was dissolved in DMAc and agitated vigorously at room temperature for 24 h under N_2 atmosphere to form PAA. Then, different amounts of Fe_3O_4 and ODA-Fe_3O_4 nanoparticles (5 and 8 mass%) were dispersed in the PAA solution by sonication overnight at room temperature. By casting the resulting mixtures on to glass petri dishes and then step heating (at each temperature of 80, 120 and 160 °C for 1 h, and 200 °C for 4 h, respectively), the PI/Fe_3O_4 and PI/ODA-Fe_3O_4 nanocomposites were obtained.

Characterization

A Unicom Galaxy Series FT-IR 5000 spectrophotometer in the region 400–4000 cm^{-1} using pressed KBr disks was used to obtain FT-IR spectra. The ^{1}H-NMR spectra were recorded on a Bruker Avance spectrometer operating at 400 MHz in DMSO-d_6 with TMS as an internal standard.

Molar mass (mass average (M_w) and number average (M_n) molecular masses) determination was performed in size exclusion chromatography (SEC) using Agilent Series 1100(Agilent, USA). A mixed eluent DMAc with 2 vol% water and LiCl (3 gL^{-1}) at a flow rate of 0.5 mL min^{-1} were used. The molar mass was calculated after calibration with poly(2-vinylpyrrolidone) standards.

The UV–visible spectrum was recorded at 25 °C in the 230–800 nm spectral regions with a Perkin Elmer Lambda 15 spectrophotometer. Photoluminescence (PL) spectra were obtained with a Fluorolog 3 (Horiba JobinYvon, USA) fluorescence spectrophotometer.

X-ray diffraction (XRD) was measured with a Philips X'Pert (Cu–Ka radiation, $\lambda = 0.15405$ nm) in the range of $2\theta = 10°$–$60°$ using 0.04° as the step length. The morphological analysis was carried out using transmission electron microscopy (TEM) with LEO 912 microscope.

The thermal stability of the samples was investigated by thermo gravimetric analysis (TG) (TA instruments Q 5000) from room temperature to 800 °C at a heating rate of 10 °C min^{-1} in nitrogen atmosphere. TA instrument Q 1000 was used to measure differential scanning calorimetry (DSC) data.

Magnetic properties were investigated using an alternating gradient force magnetometer (AGFM) device, made by Meghnatis Daghigh Kavir Co. (Kashan, Iran) in an

applied magnetic field sweeping between ±10,000 Oe. The combustion properties were analyzed by microscale combustion colorimeter (MCC).

Results and discussions

Monomer synthesis

Diamine (7) containing xanthene and amide groups was synthesized through four step reactions (Scheme 1). In the first step, the nitro compound (3) was synthesized from 4-nitrobenzaldehyde and two equivalent of 3,5-xylenol in the presence of *p*-TSA as a catalyst. For preparation of amine compound (4) palladium on charcoal (10%) and hydrazine monohydrate were used for reduction of nitro compound (3). In the next step, the amine compound (4) was reacted with 3,5-dinitrobenzoylchloride (5) and then reduced with Pd/C to the target diamine (7) produced.

Synthesis of the polyimide

The synthetic route of PI is represented in Scheme 2. New PI containing xanthene groups was synthesized from diamine (7) and epiclon (8) using two different methods. Incorporation of aliphatic and xanthene groups in the polymer backbone has been a successful approach to improve processability of aromatic polyimides without loss of their important properties such as thermal and mechanical properties.

The solubility of PI was investigated using 0.01 g of PI sample in 2 mL of solvent. Due to the presence of bulky pendent groups and flexible aliphatic units, PI had good solubility in organic solvent. The synthesized PI was dissolved in polar organic solvents such as *N,N*-dimethyl acetamide (DMAc), *N,N*-dimethyl formamide (DMF), dimethyl sulfoxide (DMSO) and *N*-methyl-2-pyrrolidone (NMP) at room temperature and it was insoluble in solvents such as chloroform, methanol, ethanol and water.

Molecular masses of the synthesized polyimides using two different methods were compared. The synthesized PI by chemical imidization exhibited number average molecular mass ($\bar{M}_n$) and weight average molecular mass ($\bar{M}_w$); 1.1×10^4 and 2.3×10^4, (poly-dispersity index (PDI) = 2.3), respectively, as measured by SEC, relative to poly(vinylpyrrolidone) (PVP) standards. The synthesized PI by thermal imidization showed higher molecular mass data, (number average molecular mass ($\bar{M}_n$) and mass average molecular mass ($\bar{M}_w$); 1.6×10^4 and 4.2×10^4, (poly-dispersity index (PDI) = 2.6), as compared with the synthesized PI by the chemical method. For preparation of the nanocomposites, thermal imidization as an efficient method was used to synthesis PI.

The chemical structure of the synthesized PI was confirmed by FT-IR and ^{1}H NMR spectroscopes. The FT-IR spectrum of PI showed the absorption bands at 1719 and 1776 cm^{-1} for the imide ring (symmetric and antisymmetric C=O stretching vibration), 1360 cm^{-1} for C–N stretching and 845 cm^{-1} for C=O bending, confirming the imide formation (Fig. 1).

Scheme 1 Synthesis route of diamine (**7**)

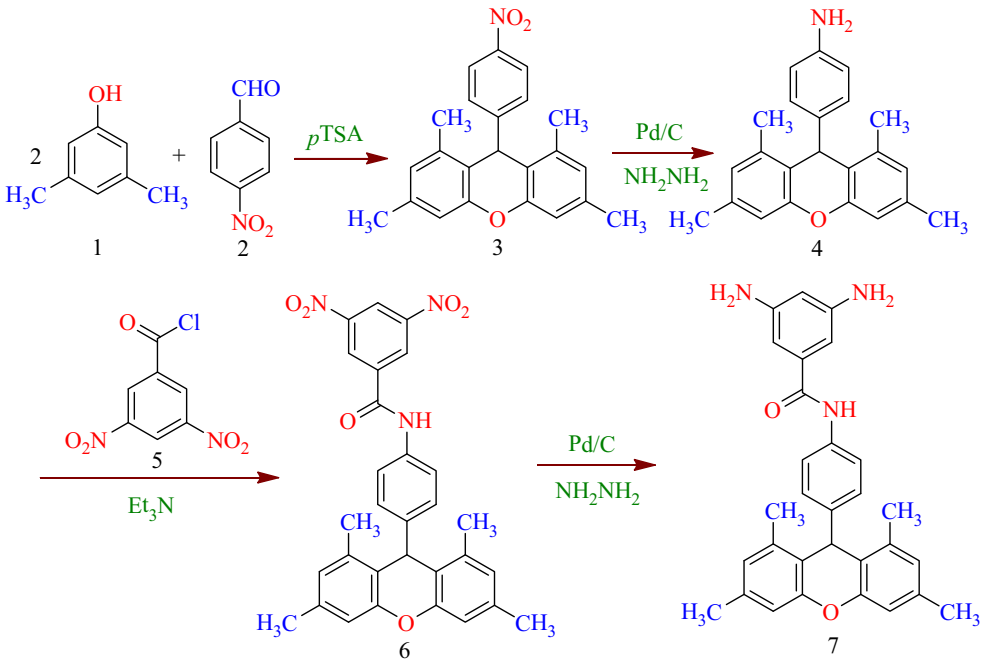

Scheme 2 Synthesis route of polyimide (**9**)

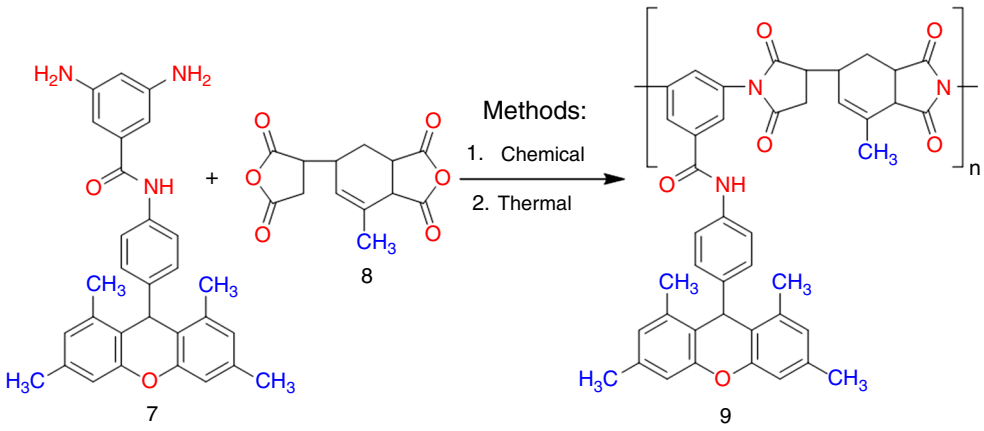

Fig. 1 FT-IR spectrum of the polyimide (**9**)

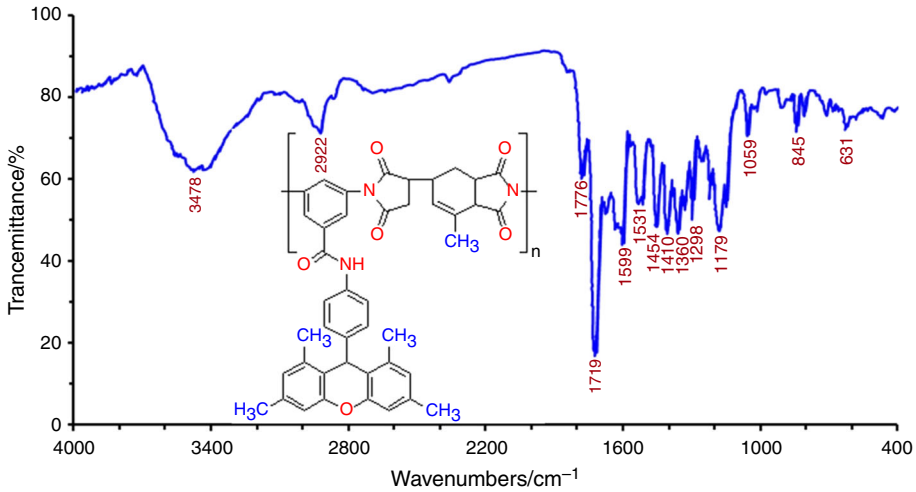

Fig. 2 ^{1}H NMR spectrum of the polyimide (**9**)

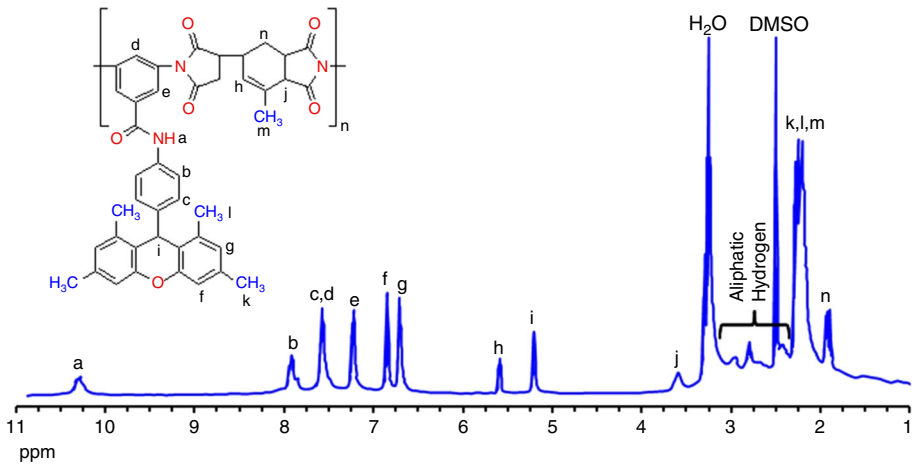

The N–H stretching vibration centered at 3478 cm^{-1} was corresponded to amide moieties, and the absorption bands at 2824 and 2922 cm^{-1} were attributed to the symmetric and antisymmetric vibrations of methene, respectively. Moreover, absorption band at 1179 cm^{-1} was assigned to the C–O vibration of xanthene group.

^{1}H NMR spectrum of the synthesized PI also confirmed the successful polymer formation (Fig. 2). The proton of the N–H amide group appeared at 10.4 ppm. The resonance of aromatic and aliphatic protons appeared in the range of 6.7–8.0 and 1.9–3.8 ppm, respectively. The resonance of olefinic proton corresponding to epiclon and CH of xanthene ring were appeared at 5.6 and 5.18 ppm, respectively.

Preparation of Fe_3O_4 magnetic nanoparticles (Fe_3O_4)

The preparation of ODA-coated Fe_3O_4 nanoparticles (ODA-Fe_3O_4) is shown in Scheme 3. Fe_3O_4 nanoparticles were prepared by the co-precipitation method from Fe^{2+} and Fe^{3+} ions in basic solution and were subsequently coated with silica (Fe_3O_4@SiO_2) through the well-known Stöber method. The Fe_3O_4@SiO_2 core–shell particles were treated with 3-chloropropyltriethoxysilane (CPTS), which can bind covalently to the free-OH groups at the surface of the particles. Finally, reaction of the 3-chloropropyl-functionalized Fe_3O_4 nanoparticles (Fe_3O_4@SiO_2–Cl) with ODA afforded ODA-functionalized silica-coated magnetite nanoparticles (ODA-Fe_3O_4).

The FT-IR spectra of Fe_3O_4, Fe_3O_4@SiO_2, Fe_3O_4@SiO_2–Cl and ODA-Fe_3O_4 nanoparticles are presented in Fig. 3. FT-IR spectrum of the Fe_3O_4 nanoparticles showed the characteristic Fe–O absorption band at 575 cm^{-1} (Fig. 3A).

FT-IR spectrum of Fe_3O_4@SiO_2 showed absorption bands at 1090 and 950, attributed to the antisymmetric and symmetric stretching Si–O–Si. In-plane bending and rocking mode of the Si–O was observed at 800 and 465 cm^{-1}, respectively. The broad absorption band centered at 3410 cm^{-1} and the band at 1620 cm^{-1} were assigned to the O–H stretching vibration (Si–OH) and twisting vibration mode of H–O–H, respectively (Fig. 3B).

In the FT-IR spectrums of Fe_3O_4@SiO_2–Cl, the new absorption bands at 2926 and 2963 cm^{-1} corresponded to the symmetric and antisymmetric vibrations of methylene, confirmed the presence of the bonded alkyl groups and indicated that the functional groups were successfully grafted onto the surface of the magnetic Fe_3O_4@SiO_2 nanoparticles (Fig. 3C).

In the FT-IR spectrum of ODA-Fe_3O_4 nanoparticles the presence of N–H stretching vibration at 3400 cm^{-1} indicated that the ODA was successfully grafted onto the surface of the magnetic Fe_3O_4@SiO_2 nanoparticles (Fig. 3D).

Polyimide/Fe_3O_4 nanocomposites (PI/Fe_3O_4) (PIN-A) and polyimide/ODA-Fe_3O_4 nanocomposites (PI/ODA-Fe_3O_4) (PIN-B)

PI/Fe_3O_4 nanocomposites and PI/ODA-Fe_3O_4 nanocomposites containing 5 and 8 mass% of the nanoparticles were successfully prepared in dry DMAc through solution technique. The reaction pathway for the preparation of the nanocomposites is shown in Scheme 4.

ODA-Fe_3O_4 nanoparticles have grafted to the PI chains via bonding between N–H in amine groups of ODA-Fe_3O_4 and imide groups of PI; moreover, the presence of ether linkages corresponded to xanthene in PI chains led to more hydrogen interactions with ODA-Fe_3O_4 nanoparticles. All of the above interactions can improve physical properties of the resulting nanocomposites. The possible interactions between PI chains and ODA-Fe_3O_4 nanoparticles are shown in Scheme 5.

Characterization of the nanocomposites

Structural characterization

The XRD patterns of the neat PI, ODA-Fe_3O_4 and the nanocomposites are presented in Fig. 4. In the XRD pattern of PI, only a broad peak was observed at $2\theta = 15$–$28°$ due to a polyimide amorphous phase [27]. The XRD pattern of ODA-Fe_3O_4 revealed the characteristic reflections at $2\theta = 18.3°$, $30.2°$, $35.5°$, $37.2°$, $43.2°$, $53.6°$, and $57.1°$, that was assigned to (220), (311), (400), (422), (511), (440) and (533) crystalline planes of Fe_3O_4, respectively [28]. The broad characteristic reflection at $2\theta = 23°$ was related to the amorphous silica phase structure in the shell of the silica-coated Fe_3O_4 nanoparticles (Fe_3O_4@SiO_2) [29].

In the XRD patterns of the nanocomposites, the diffraction peaks of Fe_3O_4 can be observed at $2\theta = 37.1°$, $44.3°$, $64.4°$ and $77.3°$. The diffraction peaks became more notable with increasing the nanoparticles loading.

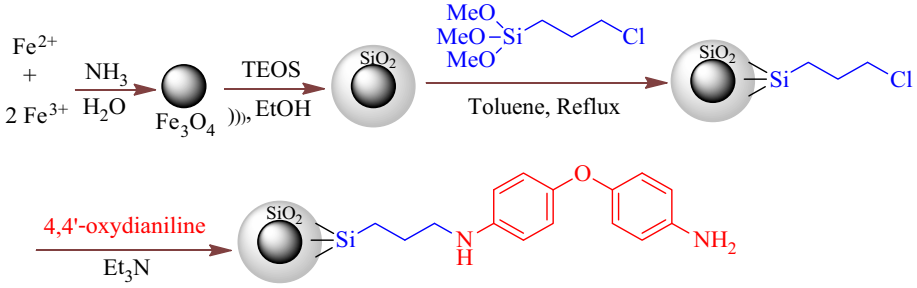

Scheme 3 Preparation of Fe_3O_4 and ODA-Fe_3O_4 nanoparticles

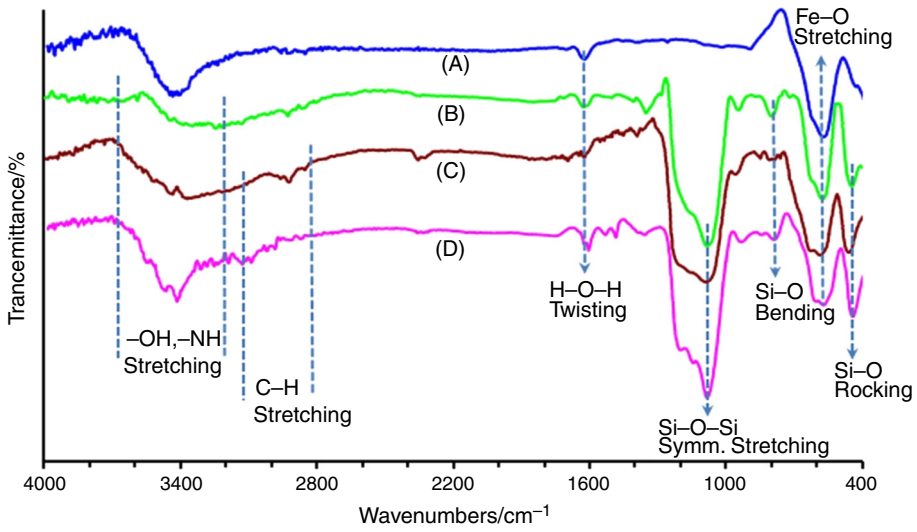

Fig. 3 Comparative FT-IR spectra for *A* Fe_3O_4, *B* Fe_3O_4@SiO_2, *C* Fe_3O_4@SiO_2–Cl and *D* ODA-Fe_3O_4 magnetic nanoparticles

As shown in Fig. 4, the intensity characteristic reflections related to Fe_3O_4 in the PI/ODA-Fe_3O_4 structure were lower as compared to the PI/Fe_3O_4 nanocomposites. This could be attributed to more chemical interactions between the PI chains and functionalized ODA-Fe_3O_4.

Morphology by TEM

The nanoscale dispersion of the Fe_3O_4 and ODA-Fe_3O_4 within the PI matrix is further corroborated with TEM analysis. The TEM images of PIN-5A and PIN-5B are presented in Fig. 5. The dark spots indicated the nanoparticles while the background corresponded to the PI matrix. The TEM image of PIN-5B showed that the ODA-Fe_3O_4 nanoparticles were more homogeneously dispersed in the PI matrix as compared with the TEM image of PIN-5A. The better dispersion of ODA-Fe_3O_4 in the PI matrix can be due to the good interfacial interactions and chemical compatibility between the PI matrix and the ODA-Fe_3O_4 structure.

Optical properties

The optical properties of PI, PI/Fe_3O_4 and PI/ODA-Fe_3O_4 nanocomposites (5 mass%) were investigated by UV–Vis and photoluminescence techniques, and corresponding spectra are presented in Fig. 6.

All the samples exhibited strong UV–Vis absorption bands with a maximum absorption (λ_{max}) at 270 nm, assignable to π–π^* transition resulting from the conjugation between the nitrogen and oxygen atoms and the aromatic rings [30, 31]. As shown in Fig. 6, the intensity absorption of PIN-5A was lower than the neat PI. It can be related to trapped electron density because of high interaction between nanoparticles and the PI chain.

The fluorescent emission of an organic structure has depended on its molecular structure and can be modified by other fluorophores functional groups in order to acquire usable properties required for special applications. Xanthene and their derivatives as a fluorophore structure have attracted great interest in recent years due to their wide range of biological and photophysical properties [32]. Photoluminescence spectra of PI and the nanocomposites showed two strong fluorescence at around 430 and 480 nm. With loading the nanoparticles in the PI matrix, the fluorescence peaks were changed to lower wavelengths which indicated some interactions between the nanoparticles and the PI chains.

Thermal properties

The thermal stability of PI, the PI/Fe_3O_4 nanocomposites and the PI/ODA-Fe_3O_4 nanocomposites was investigated by TG at a heating rate of 10 °C min^{-1}. The consequent mass losses versus operating temperature are plotted in Fig. 7. The detailed TG data, 5% (T_5) and 10% (T_{10}) mass loss temperatures and char yield are summarized in Table 1.

The TG results of PI and the nanocomposites showed two mass loss steps. The first stage, including a low amount of mass loss at $T < 275$ °C, was due to the removal of physically adsorbed solvent and surface hydroxyl groups, and the second step loss above 365 °C is related to the degradation of the main PI structure. General decomposition mass loss occurred in second step.

The TG curve of the neat PI exhibited T_5, T_{10} at 215, 279 °C, respectively, and its char yield was 28%. Considering the TG curve s of nanocomposites, it was evident that ODA-Fe_3O_4 nanoparticles had better effect than Fe_3O_4 with 8 mass% loading on the thermal properties of the

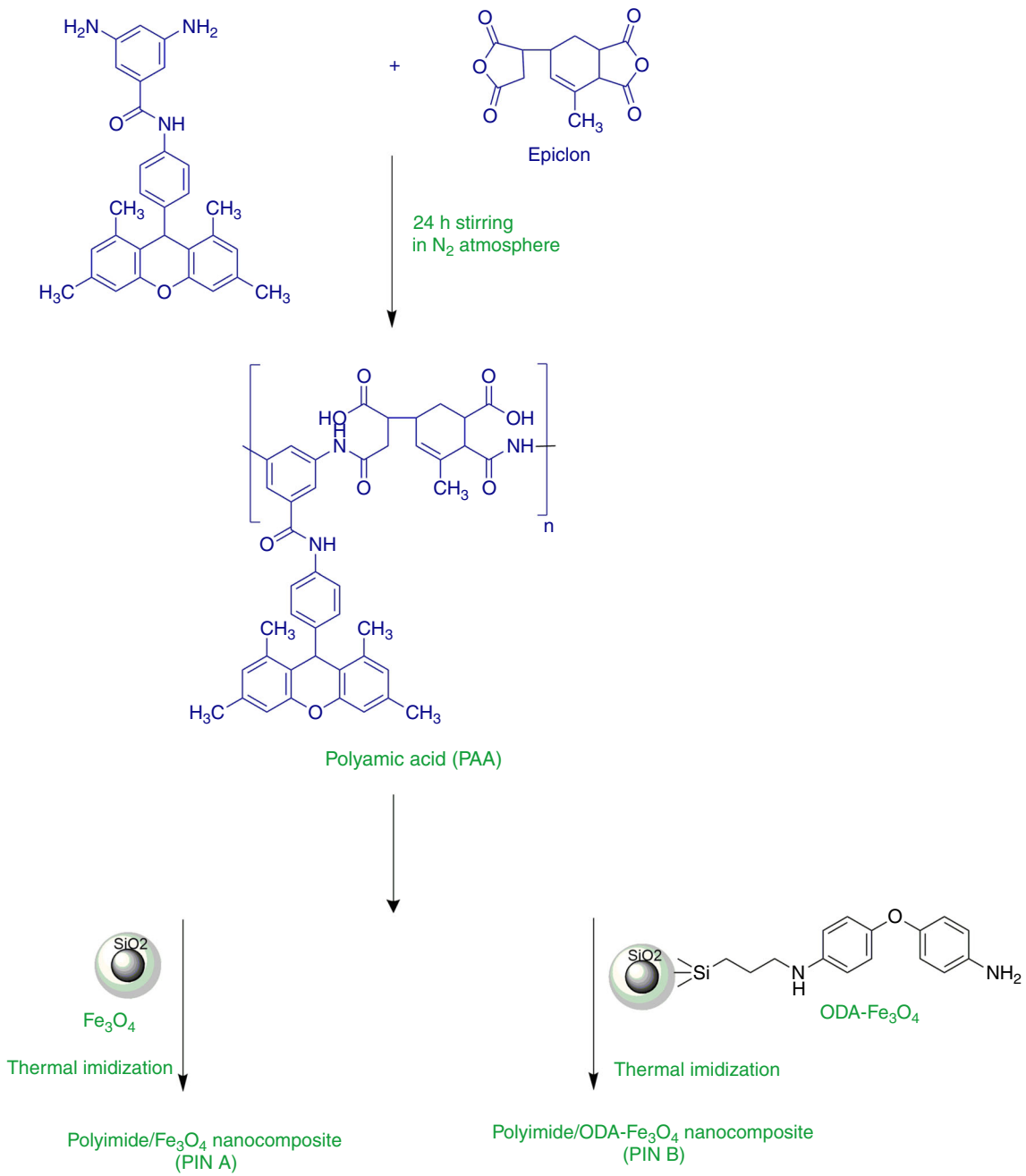

Scheme 4 Preparation of PIN-A and PIN-B nanocomposites

synthesized PI, especially in T_5 and char yield. By incorporation of 5 mass% each of nanoparticles to PI, the temperatures at 5% mass loss of PIN-A and PIN-B were slightly increased which it can be due to low interaction between the nanoparticles and the PI chain because of its low concentration. With increase in the nanoparticles contents to 8 mass%, the interactions of nanoparticles with functional groups in PI chain was better occurred and T_5 and char residues especially in PIN-B increased as compared to the nanocomposites containing 5 mass% of each the nanoparticles and the neat PI. Also, the temperatures at 10% mass loss (T_{10}) for the nanocomposites were slightly decreased as compared to PI. This could be mainly attributed to the mass loss caused by thermal degradation of organic shells on the surface of Fe_3O_4 nanoparticles.

The results of thermal analysis also showed that the residual mass at 800 °C (Char yield) has improved for NCs as compared to PI with increasing the nanoparticles contents. This improvement of char yield for the nanocomposites was attributed to the interaction between the

Scheme 5 Possible interactions between PI chains and ODA-Fe_3O_4 nanoparticles

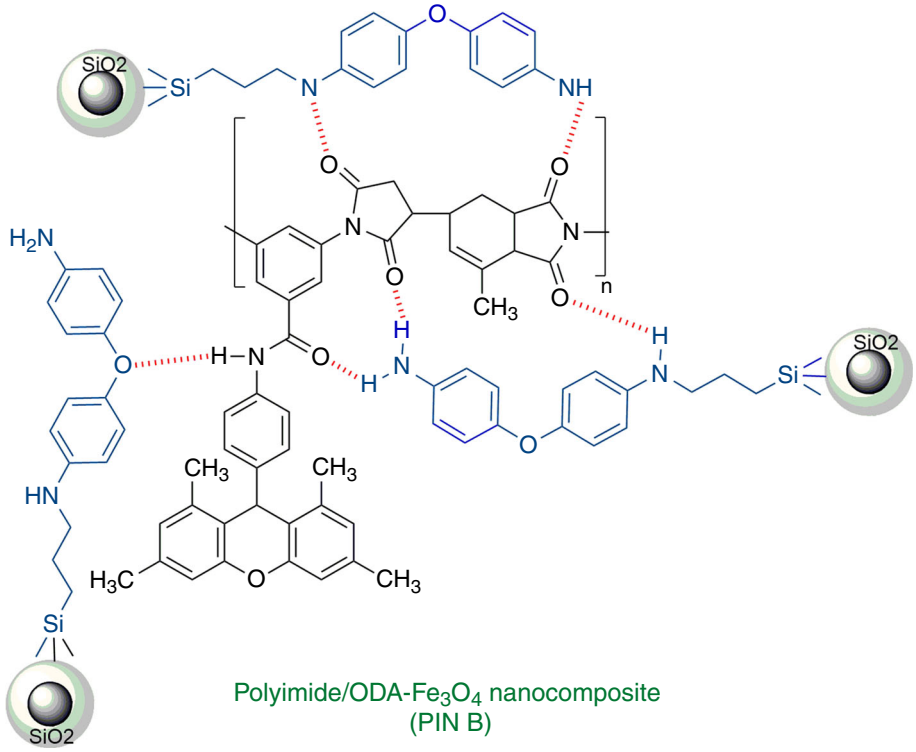

Fig. 4 XRD patterns of PI and the nanocomposites

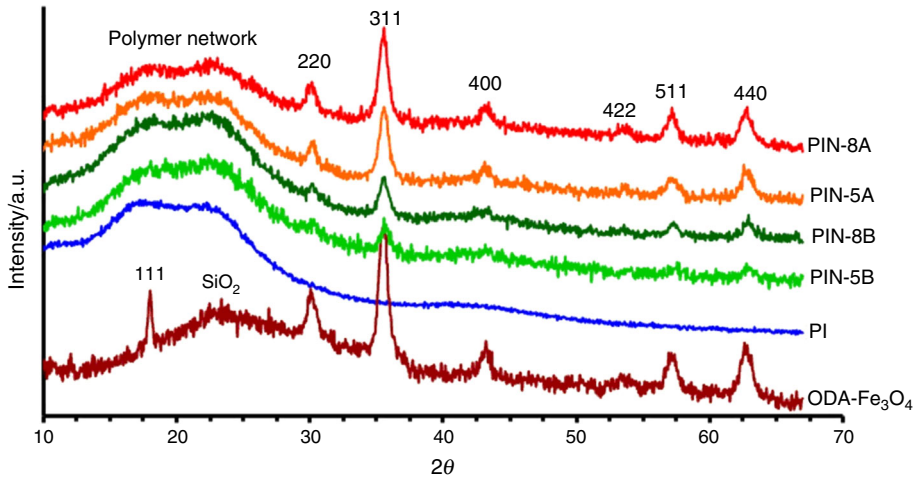

nanoparticles and the matrix at interfacial zones. The observed char yields for the PI/ODA-Fe_3O_4 nanocomposites were higher than the PI/Fe_3O_4 nanocomposites that indicated better interaction of ODA-Fe_3O_4 and PI. The results of TG confirmed the XRD and TEM results.

The glass transition temperature (T_g) of PI and the corresponding nanocomposites was measured with differential scanning calorimetry (DSC). The DSC curves are shown in Fig. 8, and the results are summarized in Table 1. The incorporation of xanthene side group and aliphatic units into the PI backbone resulted an aliphatic–aromatic polyimide with glass transition temperature (T_g) of 293 °C. A slight decrease in T_g for the nanocomposites were observed. Dispersion and interaction of nanoparticles with polymer matrix controlled T_g. This decreasing could be explained by interaction between ODA-Fe_3O_4 and the PI matrix which collapsed the interaction between the PI chains and facilitated the chains movements.

Combustion properties

In order to study the flammability of PI and the nanocomposites, microscale combustion calorimeter

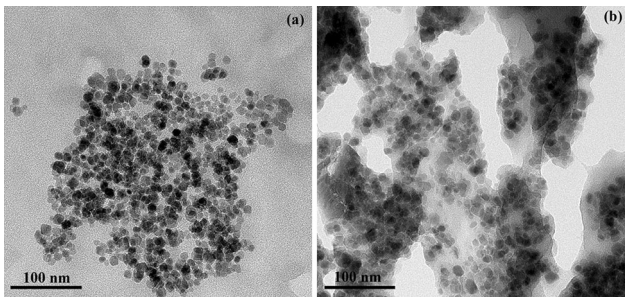

Fig. 5 TEM micrographs of (**a**) PIN-5A and (**b**) PIN-5B

(MCC) was used. The heat release rate (HRR) versus temperature is shown in Fig. 9.

The measured parameters for all the samples including heat release rate (HRR) and total heat release (THR) are reported in Table 2.

PI exhibited a peak heat release rate (pHRR) value of 231.6 W g^{-1} and THR value of 11.7 kJ g^{-1}. The pHRR and THR values of all the nanocomposites decreased as compared to the neat PI. The decrease in pHRR and THR values, suggested that the both Fe_3O_4 nanoparticles had a high efficiency on improving the flame retardancy. With

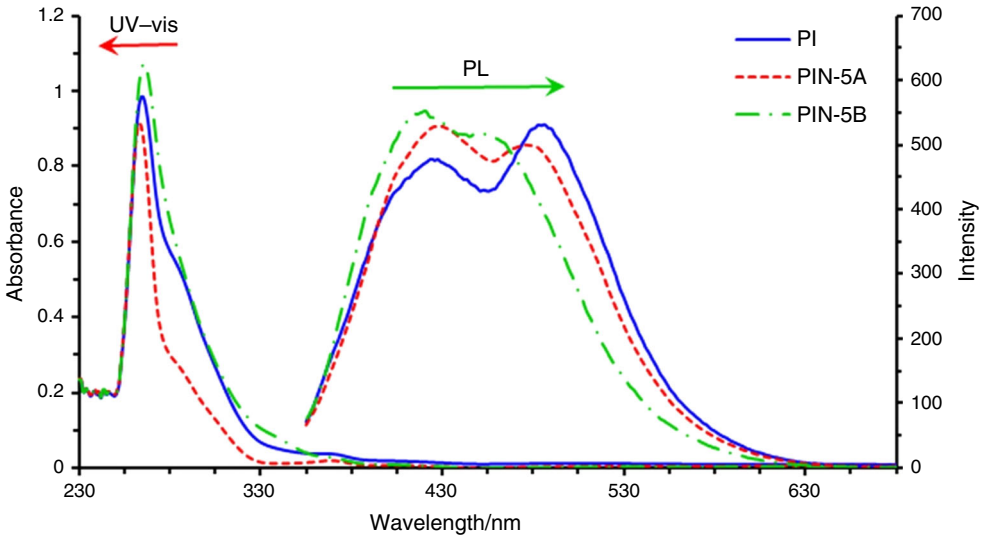

Fig. 6 UV–Vis and PL spectra of PI and the nanocomposites

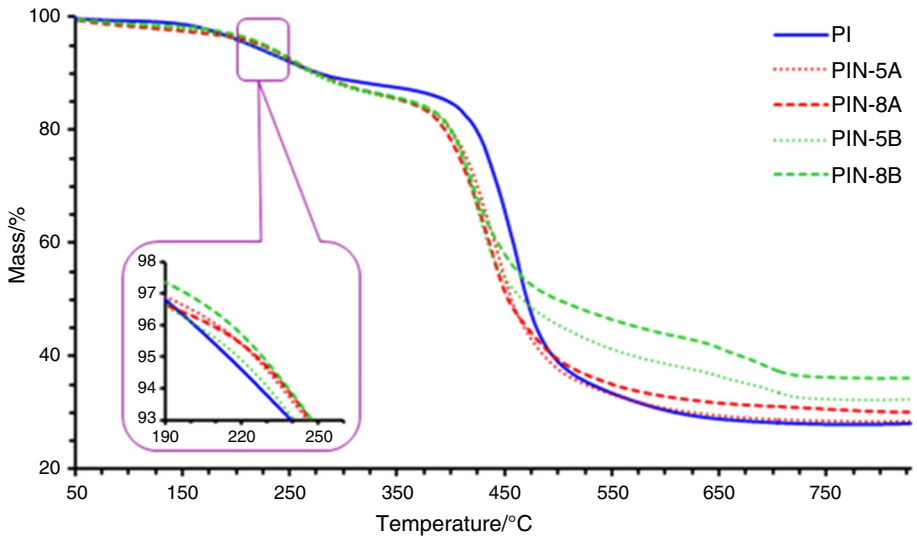

Fig. 7 TG curves of PI and the nanocomposites

Table 1 TG data of the PI and the nanocomposites

Samples	T_5/°C[a]	T_{10}/°C[a]	Char yield[b]	T_g^c
PI	215	279	28.0	293
PIN-5A	225	277	28.6	275
PIN-5B	219	271	32.5	257
PIN-8A	226	276	30.7	280
PIN-8B	229	276	36.3	250

[a] Temperature at which 5 or 10% mass loss was recorded by TG at heating rate of 10 °C min^{-1} under N_2

[b] Mass percentage of material left after TG analysis at a maximum temperature of 750 °C

[c] Glass transition temperature was recorded at a heating rate of 10 °C min^{-1} in a nitrogen atmosphere

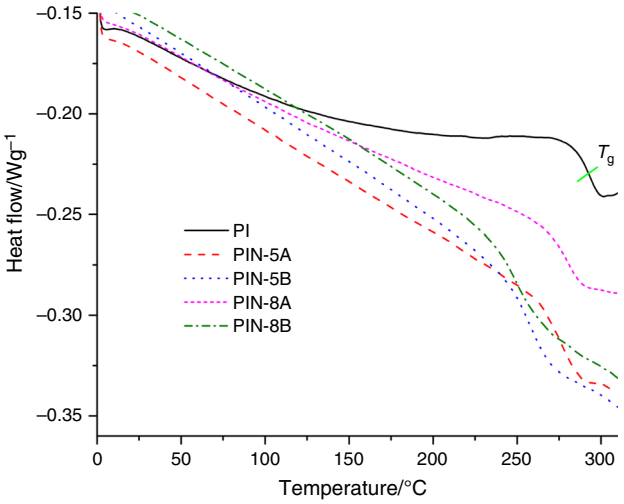

Fig. 8 DSC curves of PI and the nanocomposites

loading 5 mass% of Fe_3O_4, the pHRR and THR values were reduced. Increasing of Fe_3O_4 content up to 8 mass%, the pHRR and THR values reached to 214.7 W g^{-1} and 11.2 kJ g^{-1}, respectively. The nanocomposites based on ODA-Fe_3O_4 exhibited better results in the pHRR and THR values which indicated better protection (see Table 2). The decrease in pHRR and THR at a small amount of ODA-Fe_3O_4 was mainly attributed to slow volatilization of degradation products. The lowest pHRR value was obtained by adding 8 mass% ODA-Fe_3O_4 (pHRR = 158.1 W g^{-1}) and the lowest THR value (9.7 kJ g^{-1}) corresponded to PIN-5B. The ODA functionality of Fe_3O_4 can promote the protection of the matrix; therefore, PIN-B nanocomposites showed good flame retardancy. The difference of flammability between PIN-B and PIN-A nanocomposites was subtle.

Magnetic properties

The magnetic properties of Fe_3O_4, ODA-Fe_3O_4 and PIN-8A and PIN-8B evaluated using a vibrating sample magnetometer (VSM). Magnetization (M) versus magnetic field

Table 2 Data recorded in MCC measurements

Samples	pHRR/Wg^{-1a}	THR/kJg^{-1b}
PI	231.6	11.7
PIN-5A	221.1	10.4
PIN-5B	166.5	9.7
PIN-8A	214.7	11.2
PIN-8B	158.1	10.1

[a] Heat release rate

[b] Total heat release

Fig. 9 Heat release rate curves of PI and PIN nanocomposites

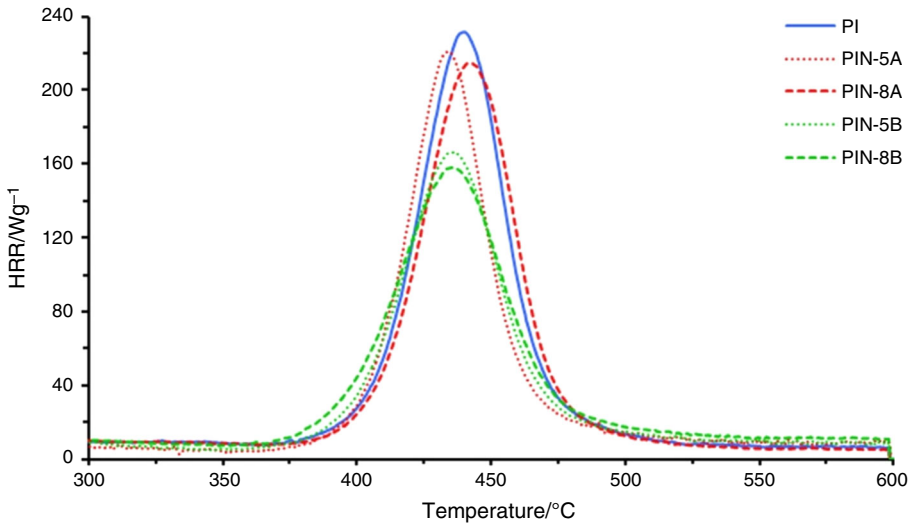

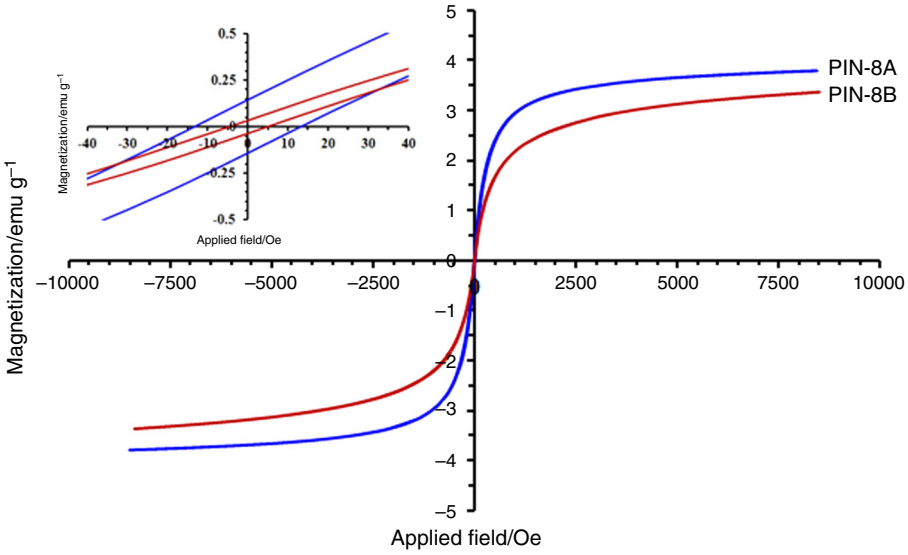

Fig. 10 Magnetization hysteresis loops of PIN-8A and PIN-8B

Table 3 Magnetic data from vibrating sample magnetometry (VSM)

Samples	M_s/emu g^{-1}[a]	M_r/emu g^{-1}[b]	H_c/Oe[c]
Fe_3O_4	53.50	1.83	25.30
ODA-Fe_3O_4	27.98	1.55	22.25
PIN-8A	3.78	0.15	13.60
PIN-8B	3.35	0.03	5.10

[a] Maturation magnetization

[b] Remanent magnetization

[c] Coercivity

(H) (magnetic hysteresis loops) of PIN-8A and PIN-8B are plotted in Fig. 10.

The hysteresis curve provides important information relative to the magnetic properties of materials including the remanent magnetization (M_r), saturation magnetization (M_s) and coercively (H_c), which are presented in Table 3.

The results indicated that the both nanocomposites had a super paramagnetic behavior at room temperature because of very insignificant coercively (H_c) and remanent magnetization (M_r) [33].

It should be noted that ferromagnetic particles with the diameter below 128 nm (a critical size) especially exhibited the characteristic of super paramagnetic material. Super paramagnetic nanoparticles tend to have a very large magnetic susceptibility but little to no H_c and M_r [34, 35].

The saturation magnetization (M_s) values of Fe_3O_4 and ODA-Fe_3O_4 are 53.50 and 27.98 emug^{-1}, respectively. M_s is defined as the state, at which point the magnetic field cannot increase the magnetization of the material further.

This reduction in M_s value for ODA-Fe_3O_4 compared to pure Fe_3O_4 is due to nonmagnetic behavior of organic shells on the surface of ODA-Fe_3O_4 and is depending on the content of organic shells [36, 37]. M_s of PIN-8A and PIN-8B was 3.78 and 3.35 emu g^{-1}, respectively, which are in agreement with M_s of ODA-Fe_3O_4 and Fe_3O_4 nanoparticles.

Conclusions

The development of polyimide/Fe_3O_4 nanocomposites was reported in this investigation. PI was synthesized using aromatic diamine containing xanthene group. The main attractive aspects of this PI were the presence of xanthene and amide groups, as well as aliphatic linkages at the polymer backbone. The structure of synthesized PI was proved by FT-IR, ^{1}H NMR spectroscopies. Surface functionalization of Fe_3O_4 with ODA not only decreased the attraction forces between nanoparticles and prevents agglomeration but also improved the interphase interaction between the nanoparticles and the PI matrix through covalent attachment of the PI chains to the ODA-Fe_3O_4 surfaces, which can further enhanced the dispersion of the nanoparticles within the PI matrix. The effect of functionalization of Fe_3O_4 on the various properties of was studied. The results showed chemical interaction between the PI chains and functionalized Fe_3O_4 nanoparticles. TEM images have also revealed better dispersion of ODA-Fe_3O_4 within the PI matrix as compared with the unmodified Fe_3O_4. Moreover, flammability and thermal properties of PI and the nanocomposites were studied by MCC, TG and DSC. TG results indicated that incorporation of 8 mass% of Fe_3O_4 NPs led to improve thermal properties of PI and also due to the presence of aromatic ring and better distribution, functionalized Fe_3O_4 NPs had better effect than the unmodified

Fe_3O_4 on thermal properties of PI. The observed Char yields for PI/ODA-Fe_3O_4 nanocomposites were higher than the PI/Fe_3O_4 nanocomposites that indicated better interaction of ODA-Fe_3O_4 and PI. According to MCC analysis, 21.8% reduction in pHRR value has been achieved by introducing 8 mass% ODA-Fe_3O_4 in the PI matrix. Magnetic properties indicated that the both nanocomposites had a super paramagnetic behavior at room temperature because of very insignificant coercivity (H_c) and remanent magnetization.

Acknowledgements This work was financially supported by grants from INSF (Iran National Science Foundation) (Grant No: 930823).

References

1. Park S, et al. Entrapment of enzyme-linked magnetic nanoparticles within poly(ethylene glycol) hydrogel microparticles prepared by photopatterning. React Funct Polym. 2009;69(5):293–9.
2. Yang C, et al. Hollow polyaniline/Fe3O4 microsphere composites: preparation, characterization, and applications in microwave absorption. React Funct Polym. 2009;69(2):137–44.
3. Yang C, et al. Synthesis and protein immobilization of monodisperse magnetic spheres with multifunctional groups. React Funct Polym. 2006;66(2):267–73.
4. Lou L, et al. Facile methods for synthesis of core–shell structured and heterostructured Fe3O4@Au nanocomposites. Appl Surf Sci. 2012;258(22):8521–6.
5. Wu W, He Q, Jiang C. Magnetic iron oxide nanoparticles: synthesis and surface functionalization strategies. Nanoscale Res Lett. 2008;3(11):397–415.
6. Mammeri F, et al. Mechanical properties of hybrid organic-inorganic materials. J Mater Chem. 2005;15(35–36):3787–811.
7. Lin J, et al. Synthesis and properties of epoxy-polyurethane/silica nanocomposites by a novel sol method and in situ solution polymerization route. Appl Surf Sci. 2014;303:67–75.
8. Sroog CE. Polyimides. Prog Polym Sci. 1991;16(4):561–694.
9. Liaw D-J, et al. Advanced polyimide materials: syntheses, physical properties and applications. Prog Polym Sci. 2012;37(7):907–74.
10. Dhara MG, Banerjee S. Fluorinated high-performance polymers: poly(arylene ether)s and aromatic polyimides containing trifluoromethyl groups. Prog Polym Sci. 2010;35(8):1022–77.
11. Sahadeva Reddy D, et al. Synthesis and characterization of soluble poly(ether imide)s based on 2,2′-bis(4-aminophenoxy)-9,9′-spirobifluorene. Polymer. 2003;44(3):557–63.
12. Qiu Z, et al. Synthesis and properties of soluble polyimides based on isomeric ditrifluoromethyl substituted 1,4-bis(4-aminophenoxy)benzene. Polymer. 2006;47(26):8444–52.
13. Lin CH, Chang SL, Cheng PW. Dietheramine from an alkaline-stable phosphinated bisphenol for soluble polyetherimides. Polymer. 2011;52(5):1249–55.
14. Kurosawa T, et al. Inducing a high twisted conformation in the polyimide structure by bulky donor moieties for the development of non-volatile memory. Eur Polym J. 2013;49(10):3377–86.
15. Maya EM, et al. Chemical modification of copolyimides with bulky pendent groups: effect of modification on solubility and thermal stability. Polym Degrad Stab. 2007;92(12):2294–9.
16. Guan Y, et al. Novel soluble polyimides derived from 2,2′-bis[4-(5-amino-2-pyridinoxy)phenyl]hexafluoropropane: preparation, characterization, and optical, dielectric properties. Polymer. 2014;55(16):3634–41.
17. Hatakeyama S, et al. A new route to substituted 3-methoxycarbonyldihydropyrans; enantioselective synthesis of (−)-methyl elenolate. J Chem Soc Chem Commun. 1988;17:1202–4.
18. Banerjee A, Mukherjee AK. Chemical aspects of santalin as a histological stain. Stain Technol. 1981;56(2):83–5.
19. Mohammad A, et al. Performance and photostability of xanthene and pyrromethene laser dyes in sol–gel phases. J Phys D Appl Phys. 2002;35(13):1473.
20. Li T, et al. A new fluorinated poly(ether amide) bearing xanthene group. Chin Chem Lett. 2010;21(10):1247–50.
21. Morisaki Y, Murakami T, Chujo Y. Synthesis and properties of [2.2]paracyclophane-layered polymers. Macromolecules. 2008;41(16):5960–3.
22. Morisaki Y, et al. [2.2]Paracyclophane-layered polymers end-capped with fluorescence quenchers. Macromolecules. 2009;42(10):3656–60.
23. Moghanian H, Mobinikhaledi A, Monjezi R. Synthesis and characterization of novel aliphatic–aromatic polyamide/Fe_3O_4 nanocomposites containing pendent 9H-xanthene groups. Des Monomers Polym. 2015;18(2):157–69.
24. Kim DK, et al. Synthesis and characterization of surfactant-coated superparamagnetic monodispersed iron oxide nanoparticles. J Magn Magn Mater. 2001;225:30–6.
25. Yu S, Chow GM. Carboxyl group (–CO_2H) functionalized ferrimagnetic iron oxide nanoparticles for potential bioapplications. J Mater Chem. 2004;14(18):2781–6.
26. Zeng T, et al. Fe_3O_4 nanoparticle-supported copper(I) pybox catalyst: magnetically recoverable catalyst for enantioselective direct-addition of terminal alkynes to imines. Org Lett. 2011;13:442–5.
27. Zhu B-K, et al. Preparation and properties of the polyimide/multi-walled carbon nanotubes (MWNTs) nanocomposites. Compos Sci Technol. 2006;66(3–4):548–54.
28. Zhang D, et al. Electrospun polyacrylonitrile nanocomposite fibers reinforced with Fe_3O_4 nanoparticles: fabrication and property analysis. Polymer. 2009;50(17):4189–98.
29. Feng G, et al. Immobilized-metal affinity chromatography adsorbent with paramagnetism and its application in purification of histidine-tagged proteins. Sep Purif Technol. 2010;74(2):253–60.
30. Schäfer AI, Akanyeti I, Semião AJC. Micropollutant sorption to membrane polymers: a review of mechanisms for estrogens. Adv Colloid Interface Sci. 2011;164(1–2):100–17.
31. Chen G, et al. Rapid and sensitive determination of plasticizer diethylhexyl phthalate in drink by diffuse reflectance UV spectroscopy coupled with membrane filtration. Food Control. 2014;35(1):218–22.
32. Singh H, Sindhu J, Khurana JM. Synthesis of novel fluorescence xanthene–aminoquinoline conjugates, determination of dipole moment and selective fluorescence chemosensor for Th4+ ions. Opt Mater. 2015;42:449–57.
33. Chantrell R, Popplewell J, Charles S. Measurements of particle size distribution parameters in ferrofluids. IEEE Trans Magn. 1978;14(5):975–7.
34. Lu A-H, Salabas EL, Schüth F. Magnetic nanoparticles: synthesis, protection, functionalization, and application. Angew Chem Int Ed. 2007;46(8):1222–44.
35. Badruddoza AZM, et al. Synthesis of carboxymethyl-β-cyclodextrin conjugated magnetic nano-adsorbent for removal of methylene blue. Colloids Surf A. 2010;367(1–3):85–95.
36. Goya GF, et al. Static and dynamic magnetic properties of spherical magnetite nanoparticles. J Appl Phys. 2003;94(5):3520–8.
37. Lin C-R, Chu Y-M, Wang S-C. Magnetic properties of magnetite nanoparticles prepared by mechanochemical reaction. Mater Lett. 2006;60(4):447–50.